

Light-scattering measurements of entropy and viscous fluctuations in a liquid far from thermal equilibrium

B. M. Law,* P. N. Segrè, R. W. Gammon, and J. V. Sengers

Institute for Physical Science and Technology, University of Maryland, College Park, Maryland 20742

(Received 11 August 1989)

We have performed small-angle Rayleigh-scattering measurements in toluene subject to a large stationary temperature gradient ∇T . The experiments demonstrate the presence of long-range entropy and viscous fluctuations enhancing and modifying the Rayleigh spectrum. The experiments confirm that the viscous-heat-mode contributions vary with $(\nabla T)^2/q^4$, where q is the wave number of the fluctuations. The observed amplitudes of both the entropy and viscous fluctuations are in excellent agreement with the theoretical predictions for the fluctuations in nonequilibrium fluids.

I. INTRODUCTION

Systems that have been removed far from equilibrium by an external field have received much attention in recent years. A good review of the status of the subject of fluctuations in a stationary external field, covering the literature up to 1984, has been given by Tremblay.¹ Here we are interested in the study of fluctuations in a steady-state temperature gradient. In the early 1970s Lekkerkerker and Boon² predicted that a temperature gradient couples the decay rates of the diffusive and viscous modes. The decay rates of the two coupled hydrodynamic viscous-heat modes are given by

$$\lambda_{\pm} = \frac{q^2}{2} \left[(\nu + D_T) \pm (\nu - D_T) \left(1 + \frac{4\nu D_T}{(\nu - D_T)^2} \frac{R}{R_c} \right)^{1/2} \right], \quad (1)$$

where q is the scattering vector, D_T the thermal diffusivity, ν the kinematic viscosity, and R/R_c the ratio of the Rayleigh number to its critical value. These coupled viscous-heat modes are *only observable for very small scattering vectors* ($q \sim 40 \text{ cm}^{-1}$) *not normally studied in conventional light scattering experiments*. Allain, Cummins, and Lallemand³ verified the critical slowing down ($\lambda_{\pm} \rightarrow 0$ as $R \rightarrow R_c$) of the viscous-heat modes on approach to the Rayleigh-Bénard instability. They created small q vectors by inducing a square-wave temperature perturbation of short duration and large wavelength ($\sim 2 \text{ mm}$) in an absorbing liquid using an Ar-ion laser. The decay of this perturbation was monitored by diffracting a cw He-Ne laser from this induced refractive index grating. Boon and co-workers^{4,5} subsequently observed propagating thermal modes (λ_{+} and λ_{-} complex) in the same geometry but with a stabilizing temperature gradient (heating from above, $R < 0$).

For conventional small-angle Rayleigh-scattering experiments, where $q \gtrsim 2000 \text{ cm}^{-1}$, the coupled hydrodynamic viscous-heat modes (1) simplify considerably. Here boundary effects can be neglected⁶ and R/R_c is given by² $R/R_c = (\alpha_T g \nabla T q_{\perp}^2 / \nu D_T q^6)$, where α_T is the thermal expansion coefficient, g the gravitational acceleration constant, and where q_{\perp} is the component of the

scattering vector perpendicular to the temperature gradient ∇T . For typical liquids and gradients $4\nu D_T R / (\nu - D_T)^2 R_c$ in (1) is much less than unity ($\sim 10^{-6}$) and to a good approximation the decay rates of the hydrodynamic modes decouple to $\lambda_{-} = D_T q^2$ and $\lambda_{+} = \nu q^2$.

We now consider the *amplitudes* of the viscous-heat modes. The mode-coupling contributions to the amplitudes of the fluctuations were incorrectly calculated in the early theoretical work of Lekkerkerker and Boon.² Kirkpatrick, Cohen, and Dorfman⁷ were the first to correctly predict the amplitudes of the fluctuations in a fluid subject to a temperature gradient using mode-coupling and kinetic theory. Ronis and Procaccia⁸ subsequently confirmed their results using fluctuating hydrodynamics. The *amplitudes* of the diffusive mode (with decay rate $D_T q^2$) and viscous mode (with decay rate νq^2) are proportional to $(\nabla T)^2/q^4$; the diffusive contribution enhances the Rayleigh line, while the coefficient of the viscous mode has a negative sign thus decreasing the correlations at shorter times. Schmitz and Cohen⁶ have calculated the full spectrum for all values of q in the regime where both the viscous and diffusive amplitudes and decay rates couple. They also included considerations of boundary effects. A simplified derivation of the Rayleigh-line enhancement and modification for a liquid in a temperature gradient with emphasis on its physical origin has been given by Law and Sengers in a previous publication.⁹

Wegdam, Keulen and Michielsen¹⁰ attempted to measure the amplitudes of the diffusive and viscous modes in the light scattering regime, but their results were subsequently shown to be in error.¹¹ We have recently reported preliminary measurements of the diffusive and viscous modes obtained with small-angle photon-correlation spectroscopy for scattering vectors where the decay rates of the diffusive and viscous modes are uncoupled.¹² We observed that the diffusive mode contribution enhanced the Rayleigh scattering, while the viscous mode contribution decreased the correlations at shorter times as predicted theoretically; both contributions were found to vary with $(\nabla T)^2/q^4$ as expected. The one remaining discrepancy between theory and experiment was in the

absolute magnitude of the enhancement: we found the experimental enhancement to be a factor of 2 smaller than predicted. This paper reports on a continuation of our earlier work in an improved cell geometry.

The paper is organized as follows. In Sec. II we review the theoretical predictions for the contributions to the Rayleigh line of a liquid in the presence of a stationary temperature gradient. In Sec. III we specify the conditions under which one optimally measures Rayleigh scattering in a nonequilibrium fluid and describe our experimental arrangement including improvements made in the design of the scattering cell. In Sec. IV we present our latest experimental results obtained with the improved scattering cell. We conclude this paper with a discussion of the results and how these results relate to recent examinations of stochastic noise sources as the initiators of hydrodynamic instabilities.

II. THEORY

As mentioned above, a number of different approaches⁶⁻⁸ have been used to calculate the mode-coupling contributions to the fluctuations in a one-component liquid subject to a stationary temperature gradient. For a simple derivation based upon fluctuating hydrodynamics the reader is referred to a previous publication.⁹ The hydrodynamic equations¹³ present a continuum description of motion in a fluid, that is, they describe the average flow of density, momentum, and energy in a fluid where any small volume element still contains a large number of molecules. The hydrodynamic equations do not describe the spontaneous fluctuations generated in a fluid as a result of molecular motion. The Onsager regression hypothesis¹⁴ states that spontaneous fluctuations "regress" back to equilibrium according to the same relaxation equations that describe the macroscopic relaxation processes. The fluctuating hydrodynamics approach to fluctuations generated by molecular motion is to supplement the hydrodynamic equations with Langevin random forces;¹³ that is, the heat transfer equation is supplemented with a random heat flux \mathbf{g} while the momentum equation is supplemented with a random stress tensor \mathbf{S} . Both of the random forces \mathbf{g} and \mathbf{S} , which represent the fast localized molecular processes, are to lowest order unaffected by the presence of a temperature gradient and thus they retain their local equilibrium correlations.¹³ As discussed in a previous publication⁹ *the enhancement and modification of the Rayleigh line for a liquid in a temperature gradient is a consequence of the coupling of fluctuations in the transverse velocity to fluctuations in the specific entropy via the temperature gradient*; this effect occurs only for scattering vectors perpendicular to the temperature gradient. The final form for the correlations in the entropy fluctuations in the frequency domain is given by⁶⁻⁹

$$\langle \delta s_{\mathbf{q},\omega} \delta s_{\mathbf{q},\omega}^* \rangle = \frac{k_B c_p q^2 D_T}{8\pi^4 \rho_0 (\omega^2 + q^4 D_T^2)} \times \left[1 + \frac{c_p v}{T_0 D_T (\omega^2 + q^4 v^2)} \left(\frac{dT}{dz} \right)^2 \right], \quad \mathbf{q} \perp \nabla T. \quad (2)$$

where k_B is Boltzmann's constant, ρ_0 and T_0 are the average density and temperature, respectively, c_p is the specific heat at constant pressure, while z is the coordinate in the direction of the temperature gradient. The corresponding time-correlation function is obtained by Fourier transforming (2)

$$C(t) = C_B \{ 1 + C_e [(1 + AP) \exp(-D_T q^2 t) - A \exp(-v q^2 t)] \}, \quad (3)$$

with

$$A = \frac{B |\nabla T|^2}{q^4}, \quad B = \frac{c_p}{T_0 (P^2 - 1) D_T^2}, \quad (4)$$

where the Prandtl number $P = \nu / D_T$.

In the heterodyne correlation function(3) a background term C_B has been included, which represents the static scattered light from all optical surfaces in the line of sight of the detector. The term C_e represents the signal-to-background ratio in the absence of any temperature gradient. From (2) it follows that

$$C_e = \frac{k_B c_p f}{4\pi^3 \rho_0},$$

where the factor f is proportional to the ratio of the intensity of the scattered light to the local-oscillator strength; it also includes a geometric term that depends upon the number of coherence areas imaged by the detector.¹⁵

For a quantitative analysis of the experiment we define an equilibrium diffusive amplitude $a_D(e) = C_e$, a nonequilibrium diffusive amplitude $a_D(n) = C_e AP$, and a nonequilibrium viscous amplitude $a_v(n) = -C_e A$, so that

$$\frac{a_D(n)}{a_D(e)} = \frac{BP |\nabla T|^2}{q^4}, \quad (5)$$

and

$$\frac{a_v(n)}{a_D(e)} = -\frac{B |\nabla T|^2}{q^4}. \quad (6)$$

There are a number of important features to be noticed about the correlation function(3) and the ratios defined in (5) and (6). The correlation function is valid only for scattering vectors \mathbf{q} that are perpendicular to the temperature gradient. The viscous mode has a negative sign which *decreases* the correlations at shorter times. Both the diffusive and viscous ratios depend upon $(\nabla T)^2 / q^4$ with the constant of proportionality being given by BP and $-B$, respectively. In our earlier work we have verified these features of the correlation function (3), except for the amplitude B whose experimental value was about half the predicted value.¹²

III. EXPERIMENT

A key feature of the correlation function (3) is the q^{-4} dependence of the new terms in the presence of a gradient; this imposes severe restrictions upon the experimental design. For readily accessible gradients ∇T of

~ 100 K/cm one must operate at scattering angles θ less than $\sim 0.75^\circ$ in order to observe both diffusive- and viscous-mode enhancements.

A schematic of the original optical arrangement used in our preliminary measurements¹² is shown in Fig. 1. It incorporated the following design features: (i) A large laser to sample cell distance (~ 3 m) in order to remove high-angle scattered light from the incident laser beam with the aid of irises; (ii) incident laser powers not more than ~ 110 mW to exclude the possibility of laser heating in the liquid sample;¹⁶ (iii) a scattering vector \mathbf{q} perpendicular to the gradient; (iv) heating from above to avoid convection; (v) the incident laser beam propagating antiparallel to the temperature gradient to avoid bending of the beam due to the large refractive-index gradient; (vi) use of a fluid layer with a small height (2 mm) so that large temperature gradients up to 260 K/cm could be obtained by applying only small temperature differences (the thermophysical properties of the liquid then do not vary significantly over the height of the cell); (vii) scattering angles θ less than 0.75° . Index matching AR-coated windows and reimaging optics enhance the signal to background by a factor of ~ 700 at these small angles; (viii) heated (cooled) gentle nitrogen-gas jets to keep the upper (lower) windows clean and also to provide thermal isolation; (ix) cross correlation of the output signal elim-

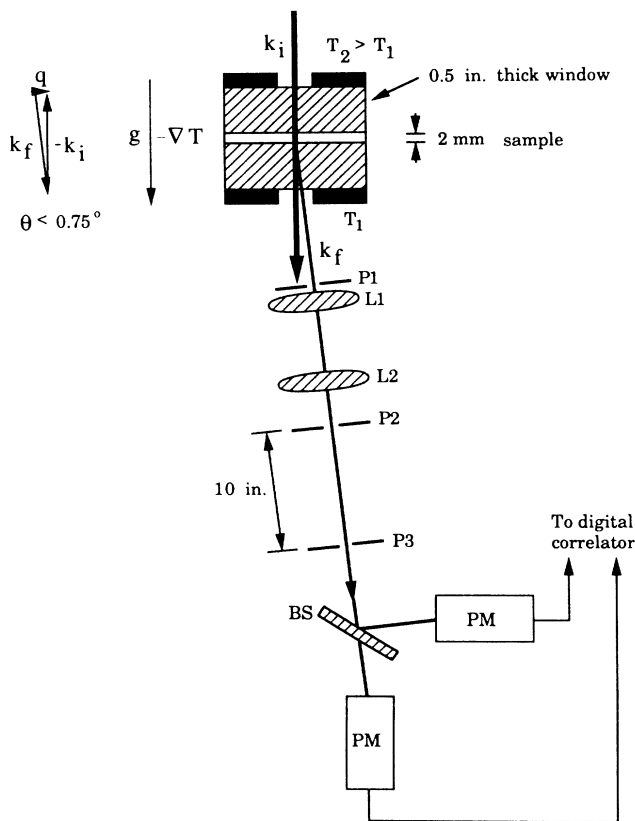


FIG. 1. Original sample cell and reimaging geometry from Ref. 12. Incident wave vector (k_i), final wave vector (k_f), pinholes (P1,P2,P3), lenses (L1,L2), beamsplitter (BS), and photomultipliers (PM).

inating the effects of afterpulsing in the photomultiplier tubes;^{17,18} (x) use of liquid toluene as the scattering fluid (toluene is a reference liquid whose thermophysical properties have been measured); and (xi) the count rate and the incident intensity were continuously monitored in order to normalize each correlation function for changes in these quantities.

Pinhole P1 (diameter 1 mm) selects the scattering direction, while lenses L1 and L2 reimage the sample cell plus window system onto pinhole P2 ($100 \mu\text{m}$) with pinhole P3 ($400 \mu\text{m}$) discriminating the dynamically scattered light from the static light scattered at the air-glass surface of both windows. The time dependence of the scattered light is determined by heterodyning with the static light. In spite of the reimaging and the use of thick windows we are still operating in the heterodyne regime; the signal to background varied from 0.05% to 3% depending upon the magnitude of the gradient and the scattering angle. A clean cell typically has a count rate of $\sim 50\,000$ counts/s for an incident power of ~ 100 mW; however, over a period of time this background count rate climbs as residual impurities are forced onto the inner cell surface due to the high radiation pressure of the strongly focused laser beam. Correlation runs last anywhere from 15 min to 2 h depending upon the magnitude of the signal to background. Two photomultipliers are used to cross correlate the output signal in order to avoid electronic correlations from afterpulsing.^{17,18} Afterpulses are created by accelerated electrons in the phototube colliding and ionizing residual gas impurities; these ionized molecules cause a correlated pulse a few microseconds after the original pulse. Afterpulses occur at random times with respect to pulses from the *other* photomultiplier; thus in the technique of cross correlation the afterpulses only contribute to the background. To align the pinholes and the optics on the scattering center the sample cell is replaced by a dummy cell, of identical dimensions, filled with a latex solution. The strongly scattered beam which propagates through pinhole P1 aids alignment of the remaining optics. The cold plate is controlled by a Forma 2095 recirculating water bath, and the hot plate by regulating the current in an electrical heater; both hot and cold copper plates are stable to within ± 10 mK over the collection time of a correlation function. Each gradient is allowed to stabilize for 3 h before data are collected on a 144-channel digital correlator (Langley-Ford 1096).

There are two limitations with the original design shown in Fig. 1. The temperature can only be measured at the hot and cold copper plates and therefore the temperature gradient across the liquid must be obtained by thermal modeling through the glass windows. Furthermore, the thin circular layer containing the liquid (Wilmad Glass Co., WG-37, pathlength 2 mm) also connected to a tipped-off glass filling stem containing a vapor bubble. This stem destroyed the cylindrical symmetry; the tip was essentially at ambient temperature thus creating a large unwanted transverse gradient in the sample cell. We believe this caused the discrepancy between the experimental and theoretical amplitudes. The transverse gradient may also have created some convective flow in

the liquid at larger temperature differences.

An improved cell system, shown in Fig. 2(a), has been designed to overcome the problems with the original sample cell. The optics and the experimental procedure are unchanged from the original, except for the addition of a laser stabilizer (Cambridge Research LS100) to reduce the magnitude of the 60-Hz laser power supply noise ($\sim 2\%$ rms) from our Spectra Physics 165 Ar-ion laser. Otherwise this noise would affect the correlation functions at long times.

A detailed cross section of the window construction is shown in Fig. 2(b). We describe the procedure for constructing the window because of the difficulties experienced in its preparation. The 0.5-in.-thick cylindrical glass windows have been epoxied into the cylindrical copper plates. Three beads of uv curing Norland 61 held the window flush to the copper surface [one bead is shown in Fig. 2(b)]; a coating of Norland 63, which dissolves in toluene, blocked the lower gap between the copper plate and the glass window to prevent the chemically resistant epoxy (Epo-Tek 380) from leaking out during cure. Norland 61 and 63 are optically clear epoxies, i.e., epoxies with a refractive index of 1.52 equal to that of glass. Chemical tests have shown that Epo-Tek 380 effectively resists toluene for longer than 1 yr. The layer of Epo-Tek 380 was applied through a syringe at a temperature of 100°C because this epoxy is thermotropic at room temperature; one must be careful not to heat the

epoxy above 120°C at which temperature it cures in 5 min. The Epo-Tek 380 was cured at 80°C over a period of 3 h. The remaining gap between the copper plate and the glass window was filled with the thermally conductive epoxy Omegabond 101 and cured at 50°C overnight. Finally, the coating of Norland 63 was removed by soaking in toluene.

A thin 2-mm-high glass ring and indium *O* rings seal the cell system. The grooves where the indium *O* rings are located are indicated in Fig. 2(a). To align the top and bottom windows parallel to each other the interference of the reflected beams was used, while the distance between the windows was determined by measuring the angular variation of the interference fringes.¹⁹ This gave a reproducible cell thickness to within $5\ \mu\text{m}$.

Liquid is introduced into the cell via the entrance hole. This new cell design avoids the problems of the earlier design. The cell has cylindrical symmetry and the temperature can be measured at the copper-liquid interface; however, the new design also has a number of undesirable features. Many different materials are in contact with toluene, which is a good solvent; as a consequence, it is more difficult to keep the liquid in the cell clean. To combat this problem a filtration system ($0.2\text{-}\mu\text{m}$ filter), with teflon solenoid controlled valves at the entrance and exit holes, has been installed. The cell system is filtered for 1 h ever 8 h for the duration of the experiment which may last many weeks running 24 h a day. However, the *in situ* filtering was not 100% effective as over a period of many weeks the count rate would slowly increase from $50\,000\ \text{s}^{-1}$ to a few million counts/sec. The only way to restore the count rate to its original low level would be to disassemble the sample cell and clean off the surface blemishes on the inner window surfaces with Windex followed by Spectrophotometric Grade acetone. The windows are birefringent due to stress birefringence; this is of no consequence for this experiment, but it prevents a depolarized light-scattering experiment from ever being performed in the same cell. The difference in thermal conductivity of the glass and copper means that for a nonequilibrium experiment the temperature at the center of the window is at a different temperature from the copper. We obtained the temperature distribution throughout the glass window and within the liquid cell by modeling the heat flow through the cell using a finite element analysis.²⁰ For large gradients ($\sim 260\ \text{K/cm}$) the temperature differential between the copper plate and the center of the glass window can be as high as 1.8°C ; the liquid between the glass windows is in a metastable state to convective flow. If one is sufficiently careful in setting up the gradient, that is, if one allows the gradient to stabilize slowly over a period of 3 h and avoids any sudden discontinuous changes in temperature, one can obtain stable gradients up to $\sim 260\ \text{K/cm}$. For the highest gradient obtainable ($300\ \text{K/cm}$) convective flow was always found, while for gradients above $\sim 100\ \text{K/cm}$ convective flow is self-sustaining once started. Convective flow could be recognized via any one of the following symptoms: (i) the reflected beam from the cell may appear to pulsate or oscillate, (ii) the nonequilibrium ratios (5) and (6) would drift by up to 50% over a sequence of correla-

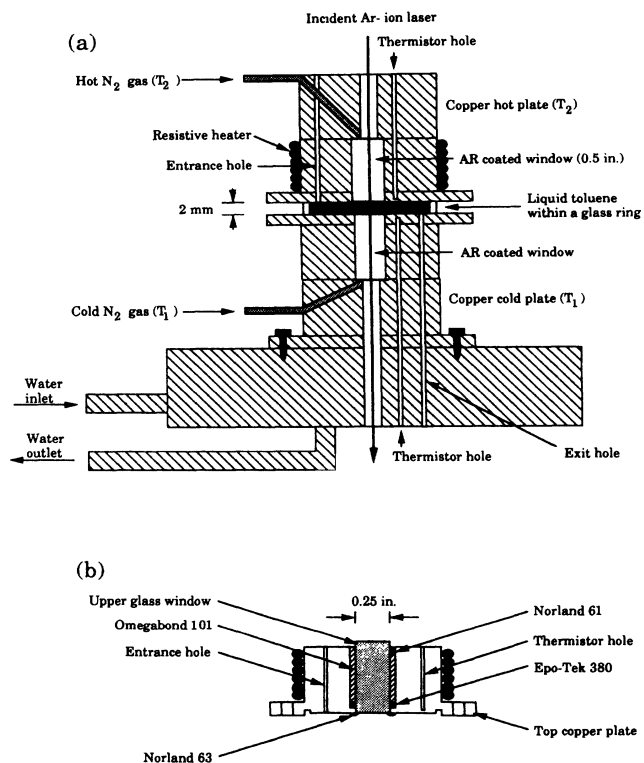


FIG. 2. (a) Modified sample cell with the 0.5-in. windows epoxied into the copper plates. (b) Detailed schematic showing the upper window construction and copper plate.

tion runs rather than be stable around some average value, or (iii) at long times on a correlogram (sample time 0.1 ms) one observed oscillations with a characteristic frequency of ~ 500 Hz (at a scattering angle of 0.67°) corresponding to liquid flow velocities of ~ 1.5 cm/s. The incident beam and the strong local oscillator from the top air-glass surface create interference fringes within the liquid (a velocimeter²¹); fluid motion perpendicular to the fringes creates oscillations in the correlogram.

In this cell one must be very careful to exclude vapor bubbles from the cell; the presence of a bubble will cause eddy patterns in the vicinity of the bubble. The top of the bubble is at a high temperature (lower surface tension), while the bottom of the bubble is at a low temperature (higher surface tension); thus the surface tension difference will drag hot material around the edge of the bubble which will consequently want to rise. High pressures within the sample cell (due to the thermal expansion of the liquid) are avoided by using friction fitted flexible teflon tubing connecting the entrance and exit holes to the solenoid valves.

IV. RESULTS

We have measured the time dependence of the scattered Rayleigh light at three different scattering angles, namely, $\theta=0.581^\circ$, $\theta=0.670^\circ$, and $\theta=0.758^\circ$. We initially obtained the data at $\theta=0.581^\circ$ and $\theta=0.758^\circ$ with a thickness $d=(2.260\pm 0.010)$ mm of the fluid layer and with temperature gradients up to 100 K/cm. We subsequently obtained a more extensive set of data at $\theta=0.670^\circ$ with $d=(2.107\pm 0.003)$ mm and temperature gradients up to 260 K/cm. In principle, we can obtain the wave number q of the fluctuations by measuring the scattering angle θ and calculate $q=(2\pi n/\lambda)\sin(\theta/2)$, where λ is the wavelength of the incident laser light and n is the refractive index of toluene. An alternative method is to determine q more directly by observing the decay rate $\Gamma=D_T q^2$ of the entropy fluctuations in the absence of any temperature gradient using the known value of the thermal diffusivity of toluene as given in Table I. Because of the smallness of the scattering angles θ , the

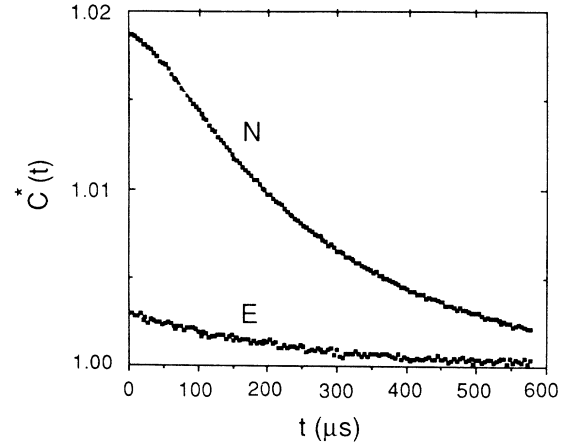


FIG. 3. Normalized experimental correlation function $C^*(t)=C(t)/C_B$ at a scattering vector of $q=2255\text{ cm}^{-1}$ demonstrating the enhancement to the diffusive mode at longer times and the decrease in the correlations at shorter times; equilibrium (E), nonequilibrium (N), with $\nabla T=220\text{ K/cm}$.

latter procedure was found to yield a higher accuracy.

In our previous experiments¹² the temperature of the toluene layer was initially 26°C . Then the toluene was subjected to increasingly larger temperature gradients by raising the temperature of the upper plate. However, this procedure has the disadvantage that the measurements corresponded to different average temperatures of the fluid layer so that the experimental data had to be corrected to correspond to the same average temperature of 26°C . In the present experiments the temperature gradient was increased by lowering and raising the temperature of the lower and upper plate, symmetrically, so that all measurements reported in this paper correspond to the same average temperature of 40°C . The scattering measurement in the absence of a temperature gradient, yielding the wave number q , was also taken at 40°C . The physical properties of toluene at 40°C , needed for the analysis of the experimental data are presented in Table I.

Typical normalized experimental correlation functions $C^*(t)=C(t)/C_B$ are shown in Fig. 3 for a scattering vec-

TABLE I. Properties of toluene at 40°C .

Thermal conductivity ^a	$\kappa=0.1266\text{ W m}^{-1}\text{ K}^{-1}$
Density ^b	$\rho=848.4\text{ kg m}^{-3}$
Isobaric specific heat ^c	$c_p=1.754\text{ kJ kg}^{-1}\text{ K}^{-1}$
Thermal diffusivity	$D_T=\kappa/\rho c_p=0.851\times 10^{-3}\text{ cm}^2\text{ s}^{-1}$
Shear viscosity ^d	$\eta=468.0\text{ }\mu\text{Pa s}$
Kinematic viscosity	$\nu=\eta/\rho=5.516\times 10^{-3}\text{ cm}^2\text{ s}^{-1}$
Prandtl number	$P=\nu/D_T=6.482$
Refractive index ^e	$n=1.497$
Fluctuation amplitude	$B=c_p/T(P^2-1)D_T^2=1.886\times 10^9\text{ cm}^{-2}\text{ K}^{-2}$

^aReference 22.

^bReference 23.

^cReference 24.

^dReference 25.

^eReference 26.

tor $q = 2255 \text{ cm}^{-1}$ in equilibrium (E) and for a temperature gradient of $\nabla T = 220 \text{ K/cm}$ (N). These same data have been plotted on a log-linear graph in Fig. 4. At the longer time scales [Figs. 3 and 4(a)] we observe the enhancement of the diffusive mode in the presence of a temperature gradient, while at shorter times [Figs. 3 and 4(b)] we find the characteristic decrease in the correlations due to the negative coefficient of the new viscous mode in Eq. (3). The slight difference in slopes for the diffusive mode [Fig. 4(a), in the presence of (N) and absence (E) of a gradient], is due to the finite spread in scattering vectors which has a greater effect on the nonequilibrium term because of the q^{-4} dependence.

In order to quantitatively compare experiment with the theoretical correlation function (3), which describes the scattering for a single q vector, one must account for the finite spread in the scattering vectors which originates from two sources, namely the focusing of the beam on the sample and the finite collection angle ($\sim 0.1^\circ$). We accomplish this by convoluting the ideal correlation function (3) with a Gaussian beam profile¹⁶

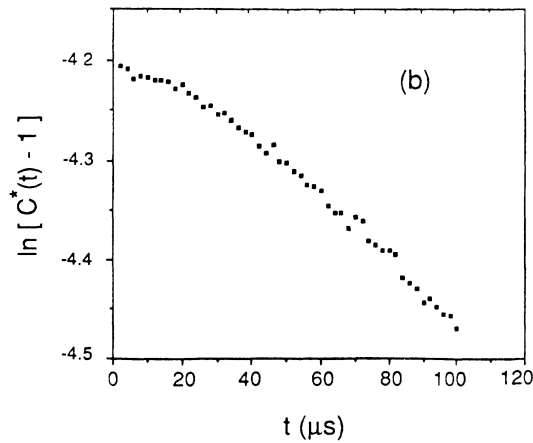
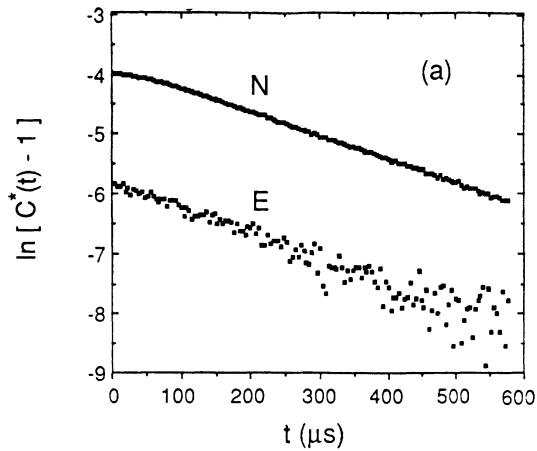


FIG. 4. Normalized experimental correlation data of Fig. 3 plotted on a log-linear graph. (a) The diffusive mode enhancement is clearly evident; $q = 2255 \text{ cm}^{-1}$, equilibrium (E), and nonequilibrium (N), with $\nabla T = 220 \text{ K/cm}$. (b) At shorter times a decrease in the correlations due to the viscous mode is observed.

$$\bar{C}(t) = \frac{1}{\sqrt{2\pi}\sigma\Phi(3/\sqrt{2})} \times \int_{q-3\sigma}^{q+3\sigma} C(t, q') \exp\left[-\frac{(q-q')^2}{2\sigma^2}\right] dq', \quad (7)$$

where q is now the average wave number, while σ is a measure of the width of the distribution of experimental wave numbers, and $\Phi(x)$ is the error function. A nonlinear least-squares fitting program, which incorporates a 10-point Gaussian-Legendre integration routine,²⁷ has been used to fit the light-scattering data. The equilibrium amplitude $a_D(e)$ and the average scattering vector q , which is related to the diffusive decay time $\tau_D = 1/(D_T q^2)$, were determined from the experimental correlation function in the absence of a gradient thus leaving only the amplitudes C_B , $a_D(n)$, and $a_v(n)$ as adjustable parameters in fitting the nonequilibrium data. In deducing these amplitudes, normalizations are made for changes in the incident intensity and the local-oscillator strength (see the Appendix). The spread σ in experimental wave numbers acts as a “global” adjustable parameter. We have confirmed that all experimental correlation functions are fitted by Eq. (7) yielding χ^2 values close to unity for a single value of $\sigma = (190 \pm 5) \text{ cm}^{-1}$, independent of both q and ∇T , thus confirming that their structure is in excellent agreement with the shape predicted theoretically for the Rayleigh line in Eq. (3). The value of σ is reasonably close to the value of $(220 \pm 20) \text{ cm}^{-1}$ calculated directly from the estimated collection angle.

The finite-collection aperture considerably broadens the nonequilibrium correlation function as is evident from Fig. 5, where we have plotted the ratio

$$R(t) = \frac{\bar{X}(t, q')}{X(t, q)}. \quad (8)$$

Here $\bar{X}(t, q')$ represents the Gaussian convolution of Eq. (7), where $C(t, q')$ on the right-hand side is replaced

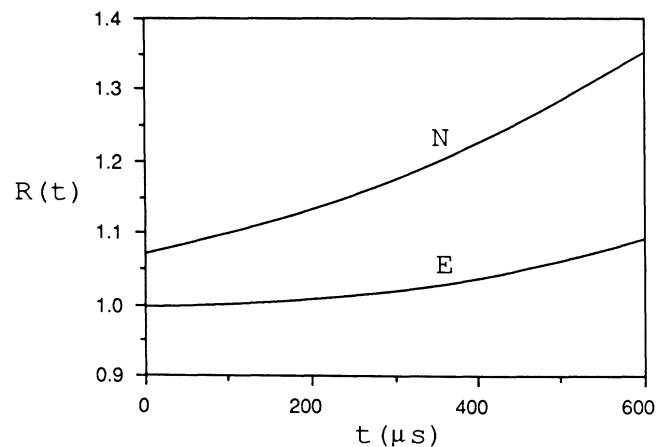


FIG. 5. Effect of a finite spread in scattering vectors q due to the finite aperture specifying the scattering angle θ . See text for the definition of the ratio $R(t)$. The equilibrium term (E) is relatively unaffected by the spread in q , while the nonequilibrium term (N) is affected at all time scales by the spread in q .

TABLE II. Nonequilibrium amplitude ratios.

∇T (K cm ⁻¹)	Heat mode			Viscous mode		
	q (cm ⁻¹)	1956±31	2255±95	2484±59	2255±95	2484±59
44.00		2.06±0.11	0.77±0.04	0.62±0.05	0.13±0.01	0.07
62.23		3.28±0.10		1.09±0.06		0.18±0.03
76.21		5.60±0.21	2.88±0.18		0.41±0.10	
88.00		7.90±0.73	3.41±0.06	2.45±0.09	0.50±0.04	0.41±0.04
98.39		8.12±0.27	4.82±0.35	2.80±0.21	0.65±0.06	0.48±0.03
120.5			7.29±0.20		1.06±0.08	
139.1			9.80±0.63		1.38±0.15	
170.4			13.30±0.26		2.15±0.05	
220.0			22.87±0.29		3.68±0.04	
260.3			30.00±1.28		4.75±0.28	

by $X(t, q')$. For the equilibrium term, $X(t, q') = \exp(-q'^2 D_T t)$, while for the nonequilibrium term, $X(t, q') = \exp(-q'^2 D_T t)/q'^4$. One notes that the equilibrium ratio (E) is not significantly broadened, as expected;²⁸ that is, $R(t)$ does not deviate significantly from unity except at larger times ($t \geq 2\tau_D$) when its magnitude is within 5% of the background. The nonequilibrium ratio (N) deviates significantly from unity at all time scales. The values of $R(t)$ shown in Fig. 5 have been calculated for $q = 2360 \text{ cm}^{-1}$, $D_T = 0.88 \times 10^{-3} \text{ cm}^2/\text{s}$, and $\sigma = 190 \text{ cm}^{-1}$.

In Table II we present the experimental results obtained for the diffusive ratio Eq. (5) and the viscous ratio Eq. (6). Only data for which there were no signs of convection are included in the table. Each entry in the table represents typically an average over eight nonequilibrium correlation functions taken at sample times of 2, 4, and 6 μs ; the associated error corresponds to one standard deviation in the spread of the data. The set of measurements obtained at $q = 1956 \text{ cm}^{-1}$ was the first set obtained with the new arrangement. It turns out that during this set of

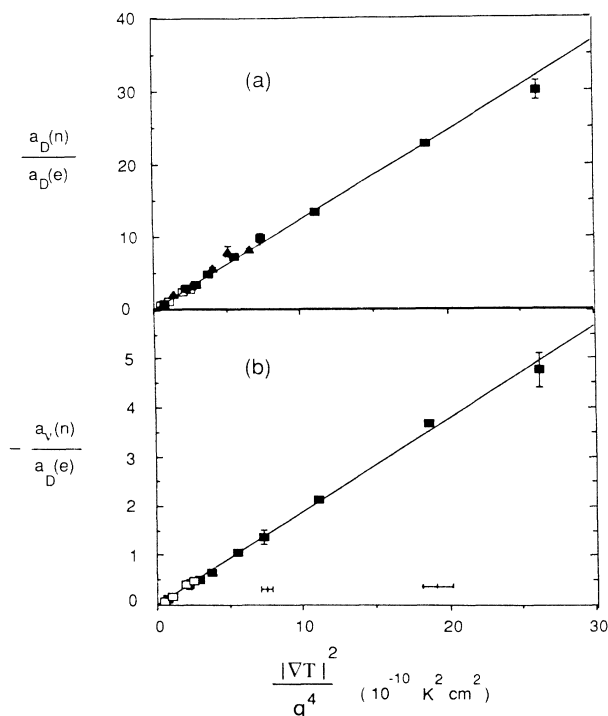


FIG. 6. Nonequilibrium amplitude ratios for (a) thermal and (b) viscous modifications to the Rayleigh line. Closed triangles, $q = 1956 \text{ cm}^{-1}$; closed squares, $q = 2255 \text{ cm}^{-1}$; open squares, $q = 2484 \text{ cm}^{-1}$. The horizontal error bars indicate the $\pm 8\%$ error in q^4 . Solid lines represent the theoretical predictions.

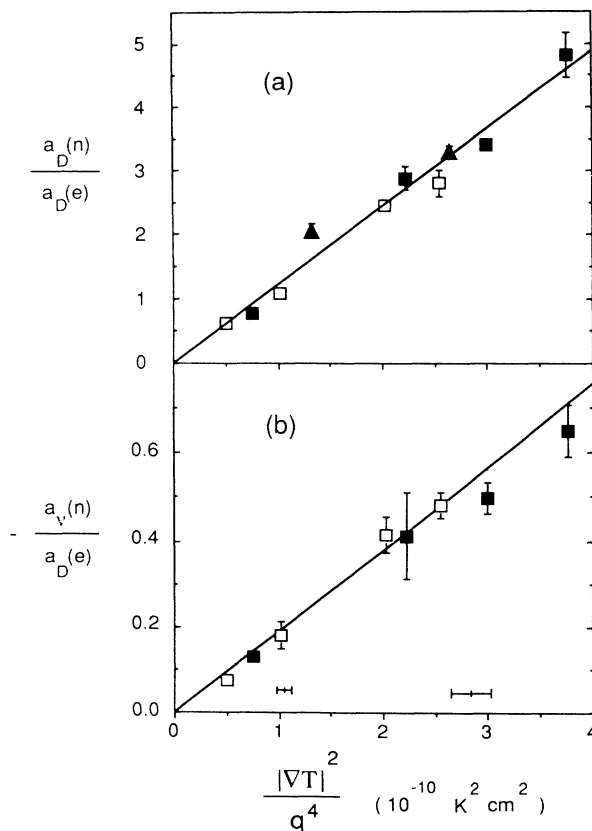


FIG. 7. Enlargement of Fig. 6 for $(\nabla T)^2/q^4$ up to $4 \times 10^{-10} \text{ K}^2 \text{ cm}^2$. The symbols have the same meaning as in Fig. 6.

measurements the delay time of the photon correlator was not optimized to yield good accuracy at shorter times. As a consequence, we do not have accurate experimental results for the contributions from the viscous fluctuations for this set of measurements. This problem was subsequently corrected.

The experimental diffusive and viscous amplitudes are plotted as a function of $(\nabla T)^2/q^4$ in Figs. 6 and 7. The complete set of data is plotted on Fig. 6. The lower end of Fig. 6 is expanded and plotted in Fig. 7. The major error in the horizontal direction in Figs. 6 and 7 is in the value of q . From the equilibrium correlation function the wave number q was determined to within $\pm 2\%$. The horizontal error bars on Figs. 6 and 7 represent the error of $\pm 8\%$ in q^4 . The solid lines represent values calculated from the theoretically predicted equations (5) and (6) without any adjustable parameters; excellent quantitative agreement is found with theory.

V. DISCUSSION

In this paper we have examined the coupling of the viscous mode to the diffusive mode which contributes to the amplitude of the Rayleigh line for a liquid in a temperature gradient and we find excellent quantitative agreement with theory. These results have important consequences for another set of nonequilibrium experiments of current interest. It has been suggested that intrinsic thermal fluctuations, such as measured in our light-scattering experiments, are the underlying noise source which initiates pattern formation in the Rayleigh-Bénard instability,²⁹⁻³¹ in dendritic growth,³² and in the Mullins-Sekerka instability.³³ However, this intrinsic thermal noise source appears to be four orders of magnitude too small to account for the onset of the instability.³¹ Thus the origin of the noise source which initiates pattern formation in these nonequilibrium instabilities remains an unresolved issue.

ACKNOWLEDGMENTS

The authors acknowledge many stimulating discussions with E. G. D. Cohen, H. Z. Cummins, and R. Schmitz. The research was supported by National Science Foundation Grant No. DMR-8814439.

APPENDIX: FITTING AND NORMALIZATION PROCEDURE

The equilibrium correlation data were fitted with C_B , $a'_D(e)$, and q as adjustable parameters, where $a'_D(e)$ is the unnormalized equilibrium amplitude. The normalized equilibrium amplitude is calculated from

$$a_D(e) = N(I, r) a'_D(e), \quad (\text{A1})$$

and then averaged over the ensemble of correlation runs taken at that angle. The normalization factor $N(I, r)$ for incident laser intensity I and average count rate r (from the two photomultiplier tubes) is given by

$$N(I, r) = \frac{I_0}{I} \frac{r}{r_0}. \quad (\text{A2})$$

I_0 and r_0 are, respectively, a conveniently chosen reference incident intensity and count rate such that $N(I, r)$ is of order unity. *The specific values chosen for I_0 and r_0 are immaterial for the amplitude ratios Eqs. (5) and (6), which are compared with theory.* The form of $N(I, r)$ is determined from the following reasoning: the count rate r can change either because the incident intensity changed or because there was additional static scattering; therefore one must determine what proportion of the count rate is due to a change in the incident intensity. We have checked that the normalized amplitude ratios calculated with Eq. (A1) are indeed independent of I and r .

Before we fit the nonequilibrium correlation data, the equilibrium amplitude $a'_D(e)$ for the specific incident intensity and count rate of the nonequilibrium experiment is calculated with the aid of Eq. (A1). The quantities q , D_T , ν , and $a'_D(e)$ are held constant in fitting the nonequilibrium light scattering data. C_B , $a'_D(n)$, and $a'_v(n)$ are adjustable parameters, where $a'_D(n)$ and $a'_v(n)$ are the unnormalized nonequilibrium amplitudes. The normalized nonequilibrium amplitudes are calculated in the same manner as Eq. (A1). The amplitudes $a_D(e)$, $a_D(n)$, and $a_v(n)$ calculated from the above procedure with the condition that σ is a global adjustable parameter, independent of ∇T and q , can now be used to calculate the amplitude ratios in Eqs. (5) and (6) for direct comparison with theory.

*Present address: Department of Physics, Kansas State University, Manhattan, KS 66506.

¹A.-M.S. Tremblay, in *Recent Developments in Nonequilibrium Thermodynamics*, Vol. 199 of *Lecture Notes in Physics*, edited by J. Casas-Vazquez, D. Jou, and G. Lebon (Springer-Verlag, Berlin, 1984), p. 267.

²H. N. W. Lekkerkerker and J. P. Boon, *Phys. Rev. A* **10**, 1355 (1974).

³C. Allain, H. Z. Cummins, and P. Lallemand, *J. Phys. Lett. (Paris)* **39**, L473 (1978).

⁴J. P. Boon, C. Allain, and P. Lallemand, *Phys. Rev. Lett.* **43**, 199 (1979).

⁵P. Lallemand and C. Allain, *J. Phys. (Paris)* **41**, 1 (1980).

⁶R. Schmitz and E. G. D. Cohen, *J. Stat. Phys.* **39**, 285 (1985);

40, 431 (1985).

⁷T. R. Kirkpatrick, E. G. D. Cohen, and J. R. Dorfman, *Phys. Rev. A* **26**, 950 (1982); **26**, 972 (1982); **26**, 995 (1982).

⁸D. Ronis and I. Procaccia, *Phys. Rev. A* **26**, 1812 (1982).

⁹B. M. Law and J. V. Sengers, *J. Stat. Phys.* **57**, 531 (1989).

¹⁰G. H. Wegdam, N. M. Keulen, and J. C. F. Michielsen, *Phys. Rev. Lett.* **55**, 630 (1985).

¹¹G. H. Wegdam, N. M. Keulen, and J. C. F. Michielsen, *Phys. Rev. Lett.* **59**, 2124 (1987).

¹²B. M. Law, R. W. Gammon, and J. V. Sengers, *Phys. Rev. Lett.* **60**, 1554 (1988); also in *OSA Proceedings on Photon Correlation Techniques and Applications*, edited by J. B. Abbiss and A. E. Smart (Optical Society of America, Washington D.C., 1988), Vol. 1, p. 147.

- ¹³L. D. Landau and E. M. Lifshitz, *Fluid Mechanics* (Pergamon, Oxford, 1984).
- ¹⁴L. Onsager, *Phys. Rev.* **37**, 405 (1931); **38**, 2265 (1931).
- ¹⁵N. C. Ford, Jr., in *Dynamic Light Scattering—Applications of Photon Correlation Spectroscopy*, edited by R. Pecora (Plenum, New York, 1985), p. 7.
- ¹⁶M. Corti and V. Degiorgio, *J. Phys. C* **8**, 953 (1975).
- ¹⁷H. C. Burstyn, *Rev. Sci. Instrum.* **51**, 1431 (1980).
- ¹⁸H. C. Burstyn and J. V. Sengers, *Phys. Rev. A* **27**, 1071 (1983).
- ¹⁹M. Born and E. Wolf, *Principle of Optics*, 6th ed. (Pergamon, Oxford, 1984).
- ²⁰M. N. Ozisik, *Heat Conduction* (Wiley, New York, 1980).
- ²¹T. S. Durrani and C. A. Greated, *Laser Systems in Flow Measurement* (Plenum, New York, 1977).
- ²²C. A. Nieto de Castro, S. F. Y. Li, A. Nagashima, R. D. Trengove, and W. A. Wakeham, *J. Phys. Chem. Ref. Data* **15**, 1073 (1986).
- ²³H. Kashiwagi, T. Hashimoto, Y. Tanaka, H. Kubota, and T. Makita, *Int. J. Thermophys.* **3**, 201 (1982).
- ²⁴D. W. Scott, G. B. Guthrie, J. F. Messerly, S. S. Todd, W. T. Berg, I. A. Hossenlopp, and J. P. McCullough, *J. Phys. Chem.* **66**, 911 (1962).
- ²⁵F. A. Gonçalves, K. Hamano, J. V. Sengers, and J. Kestin, *Int. J. Thermophys.* **8**, 641 (1987).
- ²⁶A. F. Forziati, *J. Res. Natl. Bur. Stand.* **44**, 373 (1950).
- ²⁷W. H. Press, B. P. Flannery, S. A. Teukolsky, and W. T. Vetterling, *Numerical Recipes* (Cambridge, London, 1986).
- ²⁸K. J. Czworniak and D. R. Jones, *J. Opt. Soc. Am.* **64**, 86 (1974).
- ²⁹G. Ahlers, M. C. Cross, P. C. Hohenberg, and S. Safran, *J. Fluid Mech.* **110**, 297 (1981).
- ³⁰G. Ahlers, C. W. Meyer, and D. S. Cannell, *J. Stat. Phys.* **54**, 1121 (1989).
- ³¹H. van Beijeren and E. G. D. Cohen, *J. Stat. Phys.* **53**, 77 (1988).
- ³²J. S. Langer, *Phys. Rev. A* **36**, 3350 (1987).
- ³³X. W. Qian, H. Chou, M. Muschol, and H. Z. Cummins, *Phys. Rev. B* **39**, 2529 (1989).

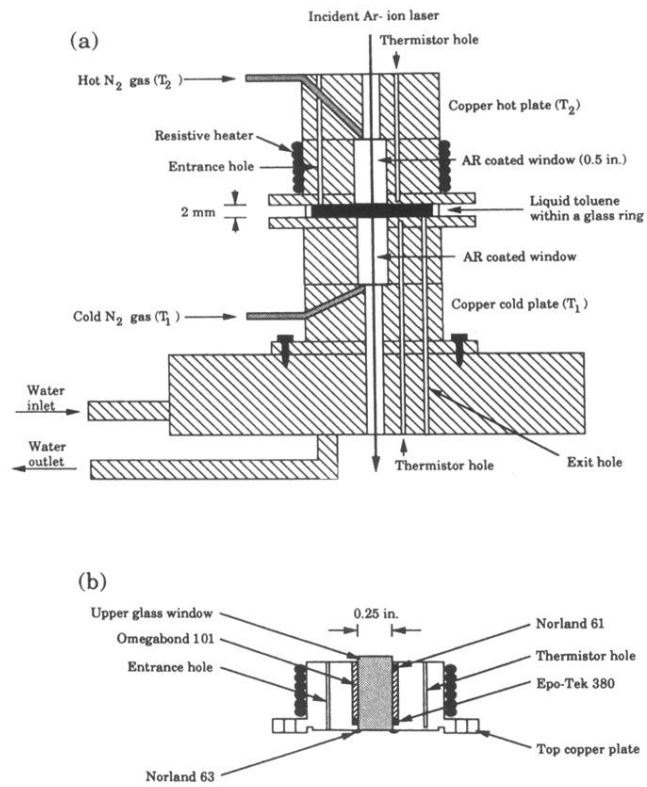


FIG. 2. (a) Modified sample cell with the 0.5-in. windows epoxied into the copper plates. (b) Detailed schematic showing the upper window construction and copper plate.